JOURNAL PRE-PROOF

This is an early version of the article, published prior to copyediting, typesetting, and editorial correction. The manuscript has been accepted for publication and is now available online to ensure early dissemination, author visibility, and citation tracking prior to the formal issue publication.

It has not undergone final language verification, formatting, or technical editing by the journal's editorial team. Content is subject to change in the final Version of Record.

To differentiate this version, it is marked as "PRE-PROOF PUBLICATION" and should be cited with the provided DOI. A visible watermark on each page indicates its preliminary status.

The final version will appear in a regular issue of *Archives of Acoustics*, with final metadata, layout, and pagination.

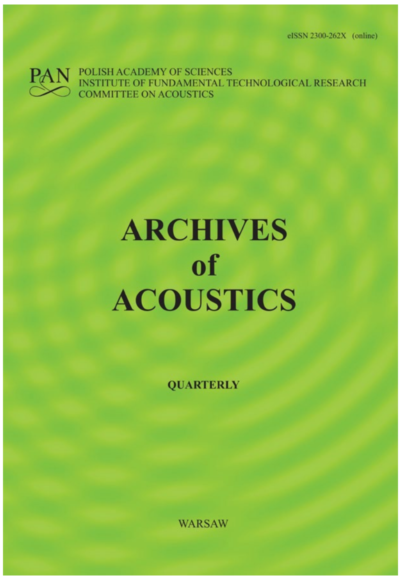

Title: Design and analysis of an ultrasonic extensive circular plate with stepped profile for special using in drying applications

Author(s): Hossein Golbakhshi, Moslem Namjoo

DOI: https://doi.org/10.24423/archacoust.2026.4469

Journal: *Archives of Acoustics*

ISSN: 0137-5075, e-ISSN: 2300-262X

Publication status: In press

Received: 2026-03-18

Revised: 2026-07-18

Accepted: 2026-08-28

Published pre-proof: 2026-09-03

Please cite this article as:

Golbakhshi H., Namjoo M. (2026), Design and analysis of an ultrasonic extensive circular plate with stepped profile for special using in drying applications, *Archives of Acoustics*, https://doi.org/10.24423/archacoust.2026.4469

Design and analysis of an ultrasonic extensive circular plate with stepped profile for special using in drying applications

Hossein Golbakhshi[1], Moslem Namjoo[2*]

[1] Department of Mechanical Engineering, University of Jiroft, Jiroft, Iran

[2] Department of Mechanical Engineering of Biosystems, Faculty of Agriculture, University of Jiroft, Jiroft, Iran

*Corresponding Author: m.namjoo@ujiroft.ac.ir

The ultrasound waves are recognized as an effective green technology with outstanding potentials in various applications including the dehydration processes of food materials. However, the application of this technology is still confined at the laboratory levels due to limited power capacity of available ultrasound systems in the large-scale airborne applications. The extensive plate radiators are essential parts that can effectively increase the amplitude of oscillations generated by piezo-electric transducers and induce high-intensity acoustic pressure field in the surrounding airflow. Using an analytical model, the geometric parameters in a simple flat circular radiator were evaluated. However, this configuration propagated counter-phase radiations with diminished overall ultrasound effect. In this study, a stepped profile with specific geometrical dimensions is proposed to modify the response of excited extensive plate. The modal analysis showed that for 20,259 Hz, just close to the system's resonance frequency, the plate generated directed and focused vibrations. Furthermore, the design provided a more convenient distribution of natural frequencies to eliminate the risk of harmful interaction of mode shapes.

Keywords: Circular radiator, Modal analysis, Ultrasonic transducer, Stepped profile

1. Introduction

The partial removal of water content is an effective method for preservation of food for a more extended period of time (Namjoo, Moradi, & Niakousari, 2022). In general, up to 15% of all industrial energy is consumed for the dehydration purposes (Ghasemi et al., 2023). However, the slow processing rates in the convective drying methods affects both the quality of end-products and the thermal efficiency (Golbakhshi et al., 2024). Thus, different non-thermal methodologies have been investigated by researchers to reduce the required drying energy and improve the quality of end products. For a brief review on the conducted works in this field, one can refer to (Zhou et al., 2024) and (Li et al., 2023).

The high-power ultrasound waves in the frequency range of 20 to 100 kHz create rapid compressing and expanding waves inside the bulk of material (known as sponge effect) and effectively accelerate the rate of mass transfer during the dehydration process (Vallespir et al., 2019). The ultrasonic waves also damage the internal membranes and intensify the micro-flow of moisture from the cell walls (Huang et al., 2020; Tang et al., 2024). Furthermore, the main drawback of conventional hot-air drying method is low heat transfer rate which leads to lengthy drying time and huge energy loss; while the ultrasound waves increase the turbulence in the flow of drying air and provide higher energy transfer efficiency (B. Xu et al., 2022). Many studies showed significant contributions to the moisture diffusion and total process time, following the application of ultrasound. Perera & Alzahrani, (2021) showed that ultrasound pretreatment at ambient temperature (without heating) may effectively reduce the possibility of nutrient degradation during the main drying process. The ultrasound has also been delivered in a non-contact way to the samples in convective hot-air drying of cumin seeds (Namjoo, Moradi, Dibagar, et al., 2022; Namjoo et al., 2025), ginger slices (Namjoo et al., 2026), caraway seeds

(Namjoo et al., 2024), blackberries (Fernandes et al., 2016) and garlic (Y. Tao et al., 2018). Recently, contribution of ultrasound to microwave vacuum drying and infrared drying were investigated by (Lei et al., 2021; J. Xu et al., 2022).

A conventional ultrasonic system usually has two main components: the generator which supplies electrical high frequency alternating current to the system, and a combined acoustic field is created by several transducers (Staszewski et al., 2018). This energy conversion is always accompanied by dissipation of energy and excessive increase in temperature of the system. However, the major challenge in application of the ultrasound is transmitting the generated acoustic signals to the crops. In the common airborne drying systems, the acoustic impedances of the transducer is considerably different from the impedance of the propagation medium, and the drying food (Mason et al., 2005). Due to lower impedance of drying air, a significant proportion of generated acoustic signal are reflected at the interface with air and increase the temperature of transducer (Gallego-Juárez et al., 2010). Therefore, in air-borne drying applications, an extensive radiating surface should be used for increasing the low power capacity of transducers.

In common industrial installations, the transducers are applied with cylindrical horns or the directional ultrasonic stepped-plate radiators. A cylindrical horn amplifies the acoustic vibrations and inflicts high-intensity air pressure waves to the drying chamber, for small scale applications. The extensive surface plate radiators in combination with the forced convective drying air, act as a reflector and properly form the standing wave field with high pressure levels in a range 155 to 160 dB (Andres et al., 2018). The ultrasonic dehydration at semi-industrial stage may also be implemented by direct contact of food material with the grooved-plate transducers (Tao et al., 2018). In this approach the acoustic impedance of the plate transducer is properly matched with the impedance of food material and the effectiveness of the drying process as well as the quality of dried food are significantly improved.

The effective performance of a high-power ultrasound system strongly depends on accurate design of its components. In special case of radiating plate surface, the configuration and geometrical sizes are crucially important parameters. In this study, we first used an analytical model to determine the thickness and outer diameter of the circular extensive plate. Then a sophisticated finite element approach was implemented to develop a proper stepped profile which enables the radiator to increase the intensity of generated by the piezo-electric transducer.

2. Material and Methods

2.1. High Power Piezo-electric Transducers

The high-power ultrasonic transducers are generally assembled as a sandwich, with paired piezoelectric discs placed between two metallic blocks as shown in Fig. 1. Between the piezo-ceramics and the metal blocks there are copper-beryllium electrodes tied in parallel which are used for applying the excitation voltage. The piezo-ceramics are polarized on longitudinal direction, with the sense of polarization alternated to each piezo-ceramic to enable parallel turn on. In the current study, the transducer is composed of four electro- ceramic rings with the constructing material PZT 802 manufactured APC International, Ltd. This material has high quality factor ($Q_m \approx 2000$) which sufficiently avoids the intense nonlinear losses and heat generation, as well as depolarization under mechanical stress (Matuda & Adamowski, 1999). The main geometrical dimensions of the components (given in Fig. 1) were selected to convert 100 W power received from the generator, mechanical vibrations with 20 to 21.8 kHz frequency in the longitudinal direction. The amplitude of such vibrations may not exceed 10 micro-meters, but should be boosted by specially designed horns or plate radiators to deliver sufficient acoustic pressure field to the main drying process.

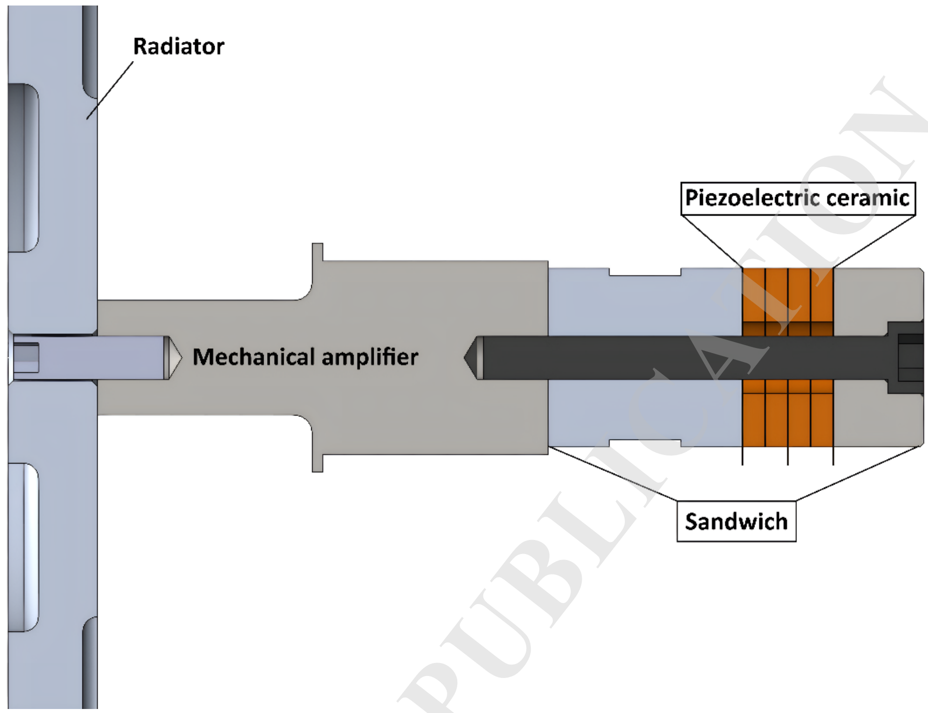

Fig. 1. The principal components in a piezo-electric ultrasound wave generating system, including the sandwich structure of transducer and basic configuration of mechanical amplifier.

Piezo-ceramic materials have more strength to compression than traction. As shown in Fig. 1, the ceramic rings are firmly compressed together by a tight bolt connection to avoid depolarization and crack during the transducer operation (Gallego-Juarez, 1989; Gallego-Juárez et al., 2010). The compression also helps to more uniform distribution of stress on ceramic discs and better thermal dissipation. The steel cylinders have an additional role to adjust the operating frequency of displacements produced by the piezo-electric discs (Andres et al., 2018).

An ultrasonic amplifier is a device used to amplify the displacements induced a high power piezo-electric transducer. This element is typically designed as a solid cylindrical body with stepped sections, where the tip has a smaller diameter. The magnification of vibrations is primarily dependent on the ratio of diameters. In addition, the extensive plate is highly desired to be driven at the resonance condition for further enhancement of the vibrations. As shown in Fig. 1, the acoustic amplifier should be fabricated without a fillet at the junction of the two cylinders (Ensminger, 1988). This limits the magnification performance and power capacity of the cylindrical stepped acoustic amplifier because of intense stress concentrations at the section with abrupt change in diameters (Amin et al., 1995). As a result, it is very difficult for the majority of existing ultrasonic transducers to satisfy all industrial requirements. The problem becomes even harder for the airborne applications due to very low density of the air. In this case, an efficient energy transmission requires a good impedance matching between the wave source and the hot airflow.

It is noted that the impedance of vibrating system is proportional to the radiating area system (Gallego-Juárez et al., 2015). Therefore, a radiator with extensive surface area enhances the radiating resistance at the interface and provides an optimal impedance matching with the medium. The radiators may be constructed as circular or rectangular plates; though other shapes might be necessary depending on the specific requirements.

2.2. The geometrical design for the extensive radiating plate

The considered radiator in this study is an extensive circular plate which should be tuned to have resonant vibrations during the operation of ultrasound dryer. The simplest design for an extensive circular radiating plate is a flat configuration with two main geometric parameters namely, the outer diameter and the thickness. A flat plate is the simplest design for the configuration of circular ultrasonic radiator. As can be seen in Fig. 1, the circular plate is attached to the tip point of mechanical amplifier by a M12 bolt, but the diameter of this bolt is considered as a fixed parameter throughout the design process. The tolerance between inner diameter of plate and the bolt is a crucial parameter and should be properly selected in the design. A loose fit allows for misalignment and harmful lateral vibration which degrades the vibration performance of transducer and creates non-uniform stresses inside PZT ceramics. According to the standard ANSI B4.1, a light interference with 0.021 tolerance is considered between the bolt and inner diameter of the radiating plate. The main role of an extensive radiating surface is increasing the amplitude of the vibrations generated by the piezo-electric transducer. So, the transverse deflection of the excited plate crucially important for convenient performance of the radiator. In a circular extensive plate with flat configuration, the external diameter and the thickness are the main geometrical sizes which should be adapted for proper dynamic vibration of the radiating plate during the operation of the system.

As a novel approach, we aim to use the results of classical theory of thin plates (Timoshenko & Woinowsky-Krieger, 1959) to choose the proper geometrical values in the initial configuration of a flat circular plate radiator and achieving the maximum possible airborne ultrasonic effect. In case of symmetrical bending oscillations which is observed during the axisymmetric vibration of the circular surface, the deflection of plate w is found from the following differential equation:

$$\frac{\partial^3 w}{\partial r^3}+\frac{1}{r^2}\frac{\partial^2 w}{\partial r^2}-\frac{1}{r}\frac{\partial w}{\partial r}=\frac{Q}{D} \tag{1}$$

where Q is the transverse shear force at the radius r, and

$$D=\frac{Eh^2}{12\left(1-\nu^2\right)} \tag{2}$$

is the bending a stiffness of the flat circular plate constructed from a material with Young's modulus E and Poisson’s ratio ν. Then if the variation of Q with r is known, Eq. (1) can be readily used to find the axisymmetric deflection of the plate. For a transducer oscillating at frequency of ω and amplitude A, the maximum transverse load applied to the inner diameter of circular plate is found from the following relation:

$$P = \rho \pi h A\left(a^2 - b^2\right)\omega^2 \quad (3)$$

where ρ is the mass density of the constructing material and h is a thickness of plate. In this case, the load P induces the following shear force on each radius of the plate:

$$Q = \frac{P}{2\pi r} \quad (4)$$

Substituting the Eqs. (3) and (4) into the differential equation (1), gives the following general solution for deflections of the circular plate:

$$w = \frac{\Pr^2}{8\pi D}\left(\ln\left(\frac{r}{a}\right) - 1\right) - C_1\frac{r^2}{4} + C_2\ln\left(\frac{r}{a}\right) + C_3 \quad (5)$$

Here C_1, C_2 and C_3 are the constants of integrations which should be determined based on the boundary conditions on inner and outer edges of circular plate. In an ideal condition, the plate the outer diameter of an extensive radiating plate should endure negligible oscillations compared to the maximum values at the middle parts. Therefore, Han et al. 2024 (Han et al., 2024) in their analytic model reduced the problem to the defamation of a circular plate loaded by a distributed load Q_0 on the inner edge r=a and fixed at outer edge r=b (see Fig. 2). We also used this boundary conditions to find the constants C_1, C_2 and C_3.

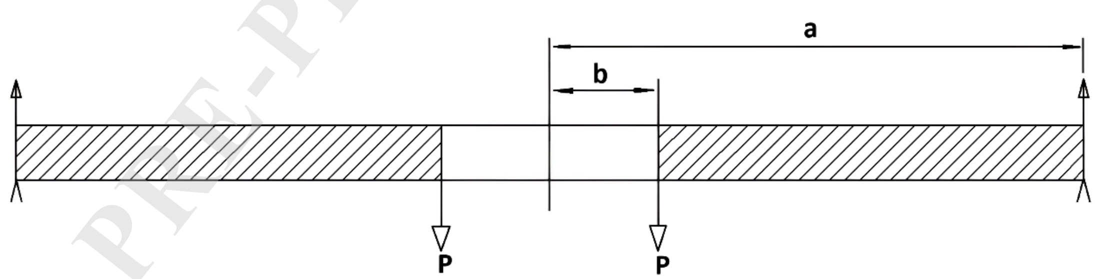

Fig. 2. The simple analytical model for analysis of loading and deflection of extensive circular plate

It is noted that the moment M_r, given by

$$M_r = -D\left(\frac{\partial^2 w}{\partial r^2} + \frac{\nu}{r}\frac{\partial w}{\partial r}\right) \tag{6}$$

is zero on both inner and outer edges. Furthermore, the outer edge is unable to deflect. As a result, the corresponding boundary conditions in this problem are as follows

$$w\big|_{r=a} = 0 \qquad M_r\big|_{r=a} = M_r\big|_{r=b} = 0 \tag{7}$$

Consequently, the three required constants are determined as

$$C_1 = \frac{P}{4\pi D}\left(\frac{1-\upsilon}{1+\upsilon} - \frac{2b^2}{a^2-b^2}\ln\left(\frac{b}{a}\right)\right) \tag{8}$$

$$C_2 = \left(\frac{1-\upsilon}{1+\upsilon}\right)\frac{P}{4\pi D}\frac{a^2b^2}{a^2-b^2}\ln\left(\frac{b}{a}\right) \tag{9}$$

$$C_3 = \frac{Pa^2}{8\pi D}\left(1 + \frac{1}{2}\frac{1-\upsilon}{1+\upsilon} - \frac{b^2}{a^2-b^2}\ln\left(\frac{b}{a}\right)\right) \tag{10}$$

Table 1. The mechanical properties of the material selected for constructing the ultrasonic radiator

Property	Value	Unite
Elastic Modulus	7.2e+10	N/m^2
Poisson's Ratio	0.33	N/A
Shear Modulus	2.69e+10	N/m^2
Mass Density	2810	kg/m^3
Tensile Strength	570000000	N/m^2
Compressive Strength		N/m^2
Yield Strength	505000000	N/m^2
Thermal Expansion Coefficient	2.36e-05	/K
Thermal Conductivity	130	W/(m·K)
Specific Heat	960	J/(kg·K)
Material Damping Ratio	N/A	

3. Results and Discussion

Based on the discussions presented in the preceding paragraphs, Eq. (5) can be used for evaluating the amplitude ratio of the flat circular radiating plate for various values of thicknesses and outer diameters. The amplitude ratio is defined as the amplitude of extensive plate vibrations to the amplitude of oscillations generated by the piezo-electric transducer. An aluminum alloy 7075-T6 with the thermo-mechanical properties given in Table 1 was selected as the constructing material. Fig. 3 illustrates the effect of thickness on the vibrating performance of the circular plate radiator. As can be seen; by decreasing the thickness of the plate, the amplitudes of ultrasound waves greatly increase. According to the obtained results, for the same outer diameter of d=380 mm, the thickness h=25 mm provides $39.21\,\%$ and $77.42\,\%$ higher amplitude ratios compared to the plates with h=35 mm and h=45 mm thicknesses, respectively.

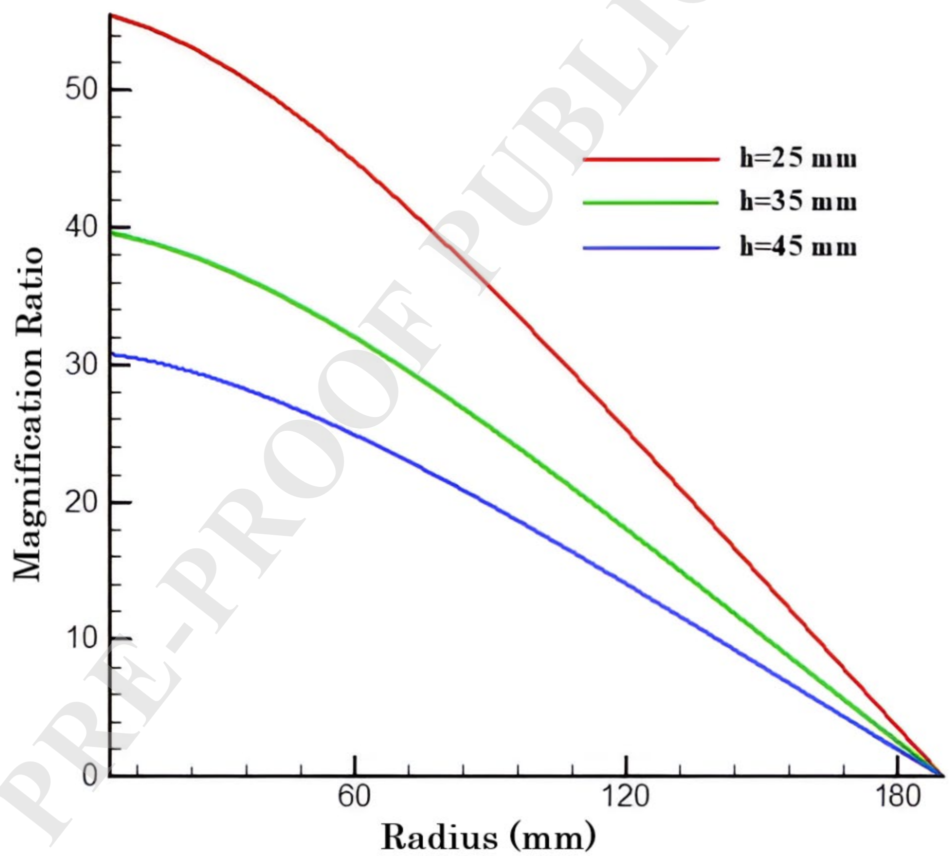

Fig. 3. Amplification performance of circular plates of same outer diameter d= 380 mm and different thicknesses.

The results of analytical mode for three outer diameters d= 340 mm, d= 360 mm and d= 380 mm are depicted in Fig. 4. In all cases the thickness was set to be a fixed value of h=25 mm. It can be easily observed that the plates with larger diameter can sufficiently radiate the waves with greater amplitudes. Then based on the results of Eq. (5), the outer diameter and the thickness of the flat circular plate are selected as 380 mm and 25 mm, respectively, for achieving the maximum possible increase in the amplitude of emitted airborne acoustic waves.

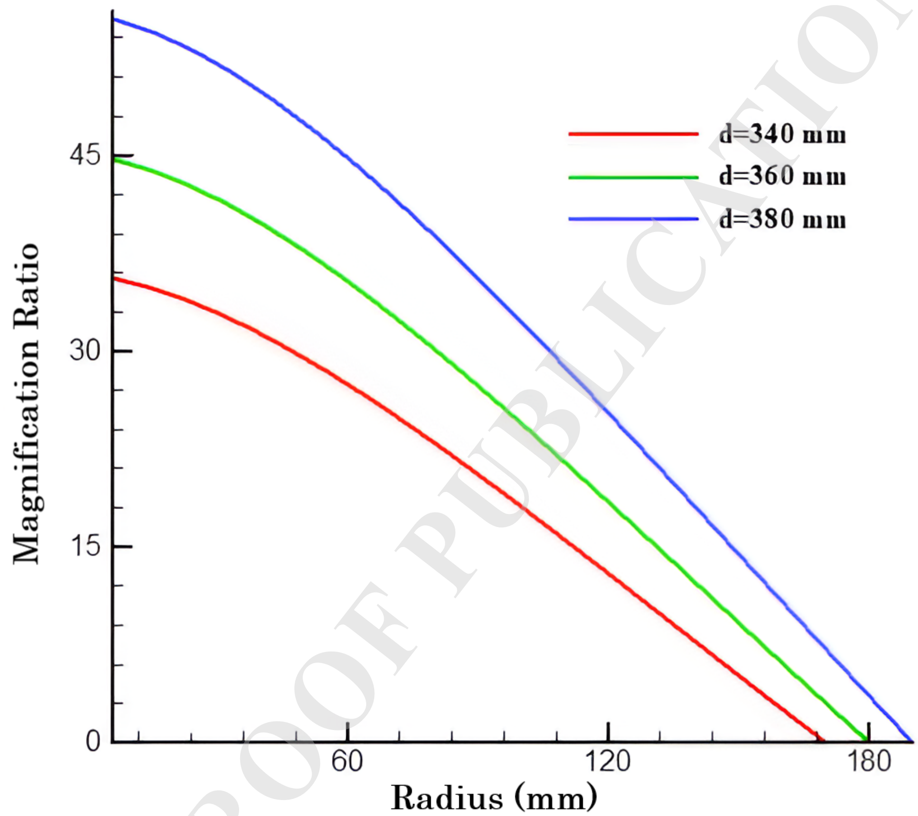

Fig. 4. Amplification performance of circular plates of same thickness h=25 mm and different outer diameter.

3.1. The mode shapes of flat circular plate

It is noted that the majority of the ultrasonic drying systems operate at the resonance frequency of $20kHz$ (Golbakhshi et al., 2024). Therefore, the extensive plate with flat configuration should have a proper vibrating behavior in a reasonable narrow bandwidth around this frequency. As an essential step in the design process of ultrasonic drying system, the modal analysis is conducted for the proposed configuration to evaluate the mode shapes near the resonance frequency of the system.

In this study, all the numerical investigations are conducted in the FEM-based COSMOS software and the results are used for more precise tuning the geometrical parameters of the extensive radiating surface. The configuration of circular plate radiator allows for using the axisymmetric mesh with flat quadrilateral elements. This provides a great reduction in computational cost of FEM analysis compared with 3D solid elements. However, the main challenge in this study refers to dealing with the steps as geometrical discontinuities which impose significant influence on the results of modal analysis. So, it is extremely crucial to refine the mesh in the step corner region. As can be seen in Fig. 10, the mesh is refined at inner and outer corners of each step. The size of elements near the steps at each stage of numerical analysis, were selected proportional to the height of steps. As can be seen in Fig. 1, the center of circular plate is connected by a bolt to the mechanical amplifier. Thus, in FEM model the inner diameter of the plate was fixed and its outer diameter was considered as free edge.

Fig. 5 shows some mode shapes of the flat circular plate near the resonance condition of the ultrasonic transducer. It is obvious that in all mode shapes that the flat shaking plate has different counter-phase oscillating zones. As a result, the radiating surface would not be able to generate focused and well-directed acoustic pressure field in the surrounding air (Gallego-Juárez et al., 2010). On the other hand, the configuration of the extensive surface has a great influence on the distribution of natural frequencies. Fig. 6 illustrates some natural frequencies of the flat circular plate near the resonance condition of the wave generating system. According to the calculations performed for the flat-type radiator, the natural frequencies with the maximum amplitudes of oscillations are found to be so close to each other. This raises the risk of modal interaction and more adverse effects on safety and performance of the ultrasound system. Thus, an alternative configuration and geometry should be selected for the extensive radiating surface.

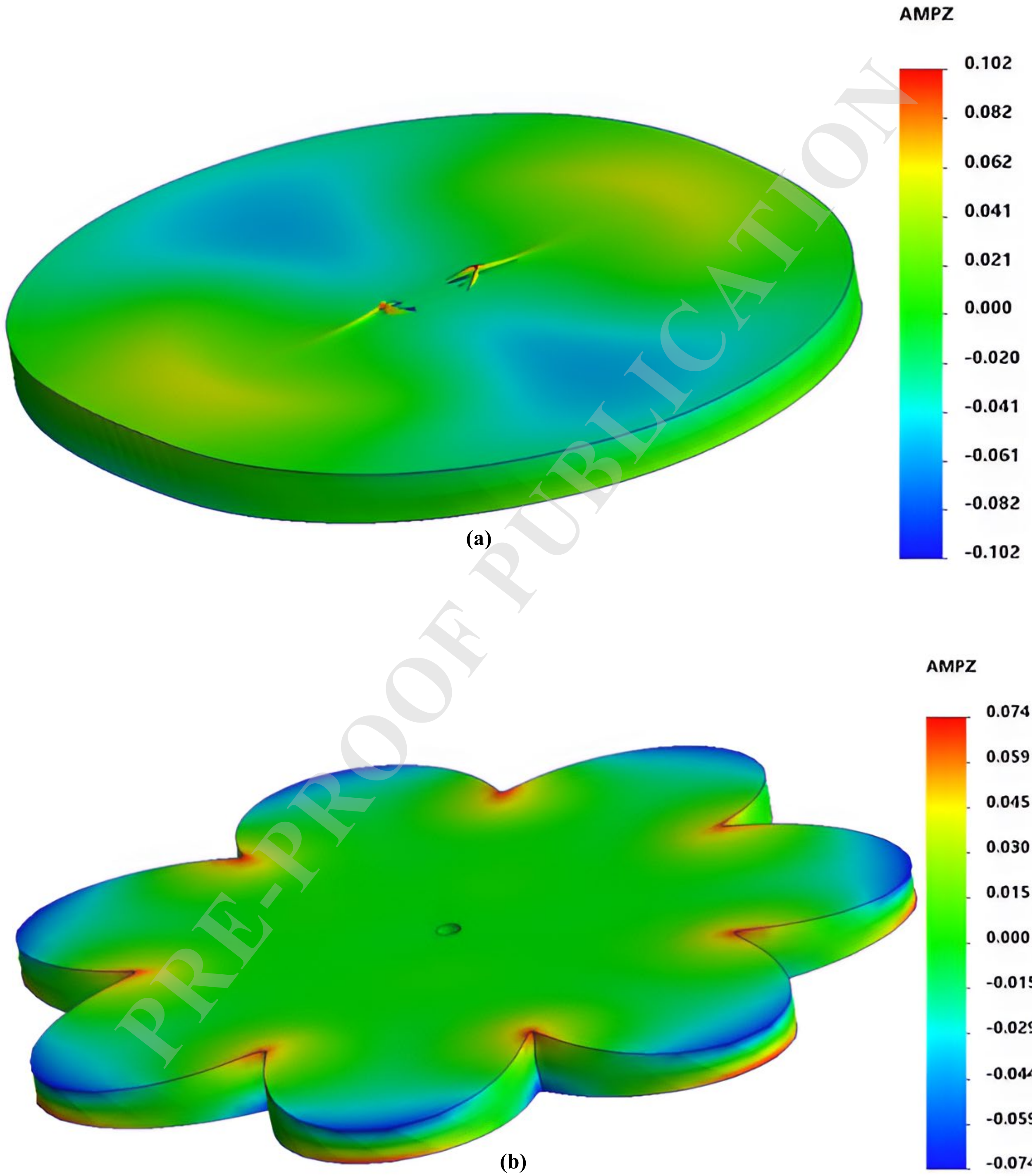

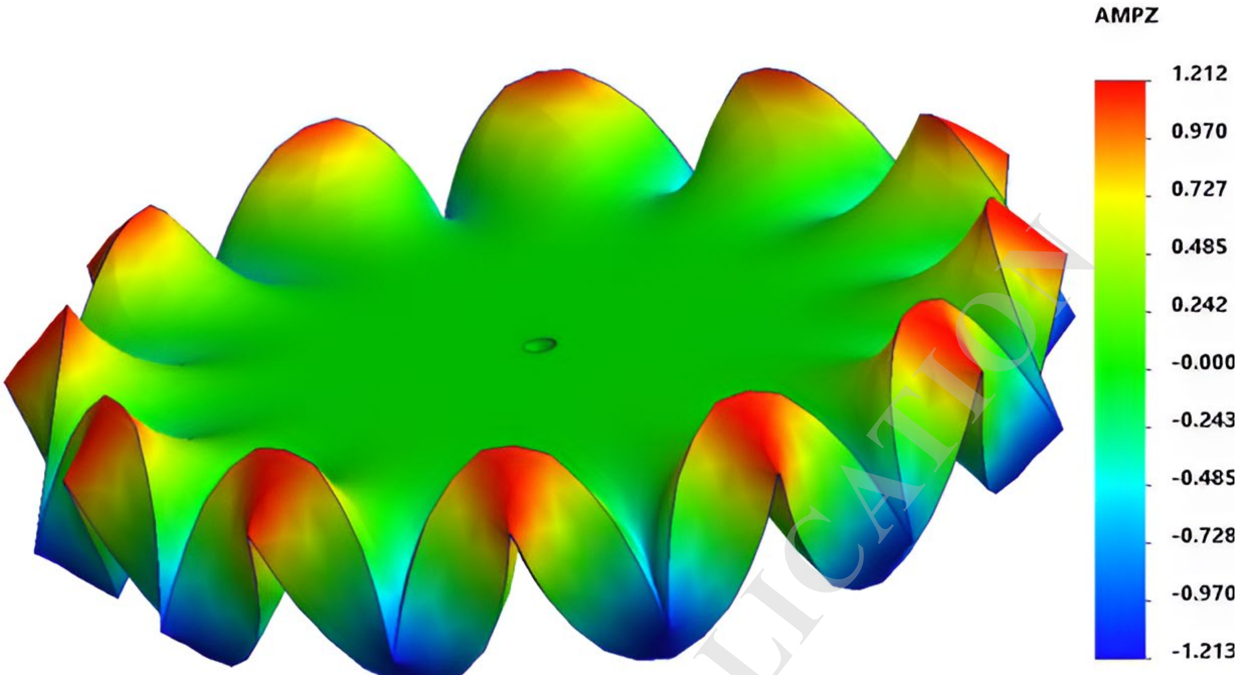
AMPZ
1.212
0.970
0.727
0.485
0.242
-0.000
-0.243
-0.485
-0.728
-0.970
-1.213

(c)

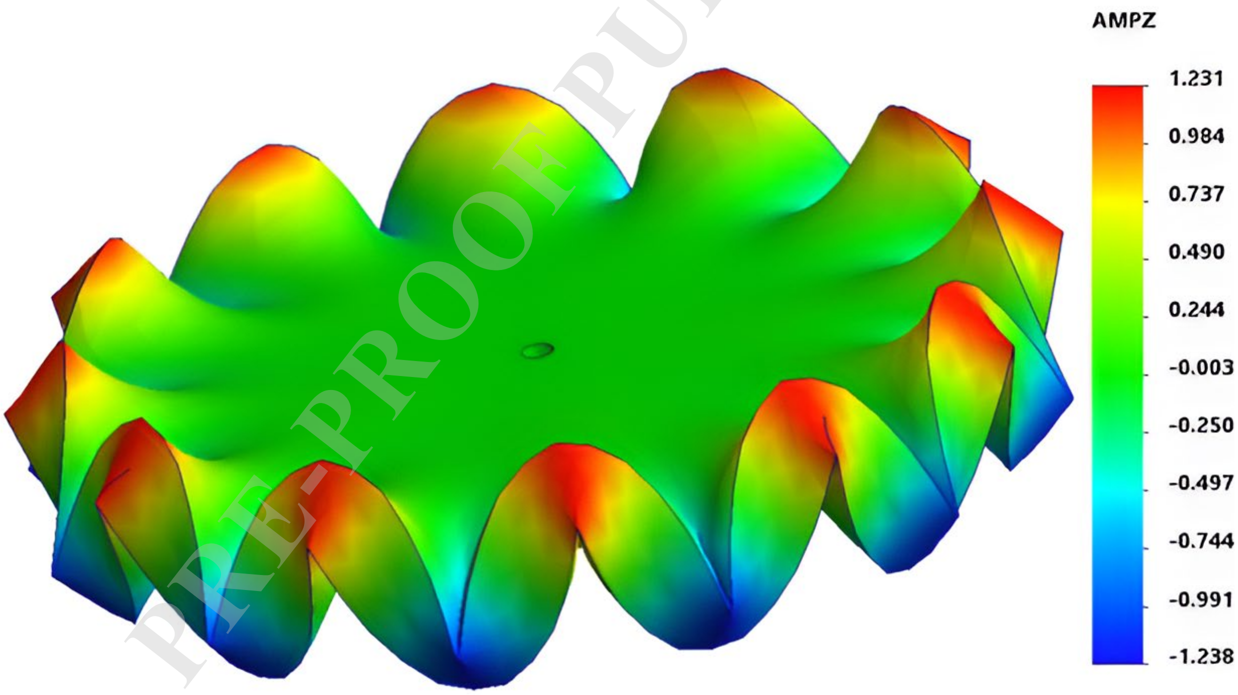
AMPZ
1.231
0.984
0.737
0.490
0.244
-0.003
-0.250
-0.497
-0.744
-0.991
-1.238

(d)

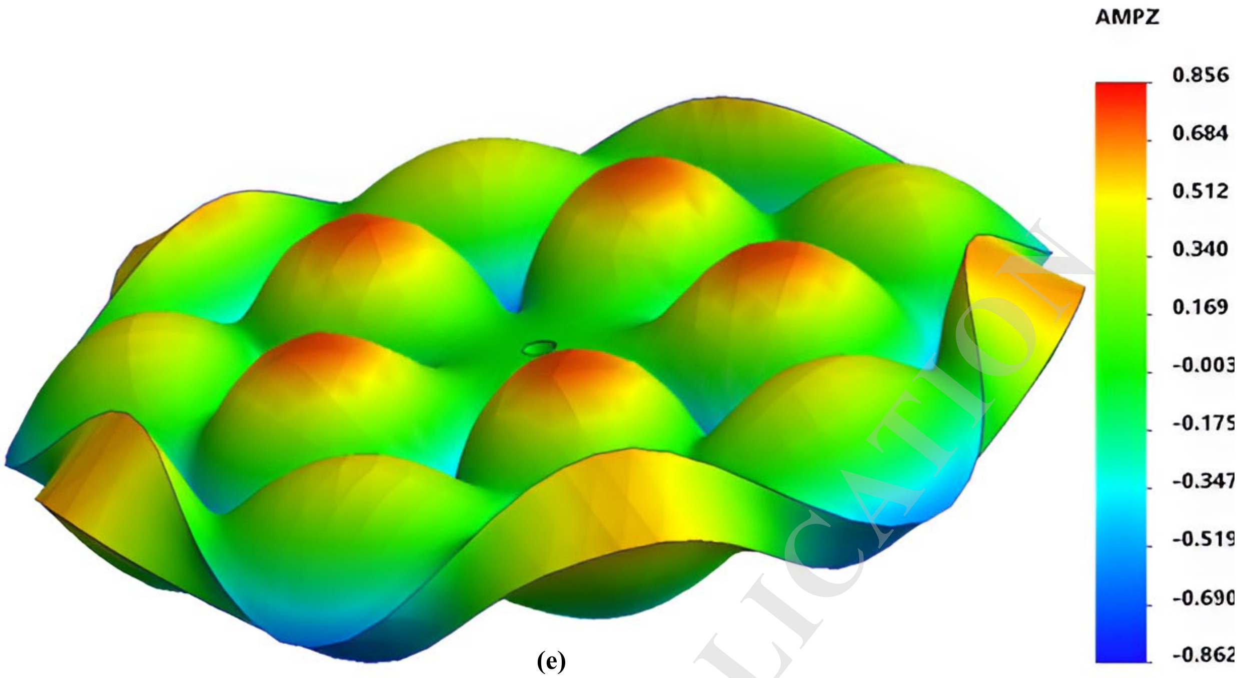

(e)

Fig. 5. Four mode shapes of resonant vibrating flat plate near the working frequacy of ultrasound drying system: (a) 19396 Hz, (b) 19591 Hz, (c) 20089 Hz, (d) 20099 Hz and (e) 20455 Hz.

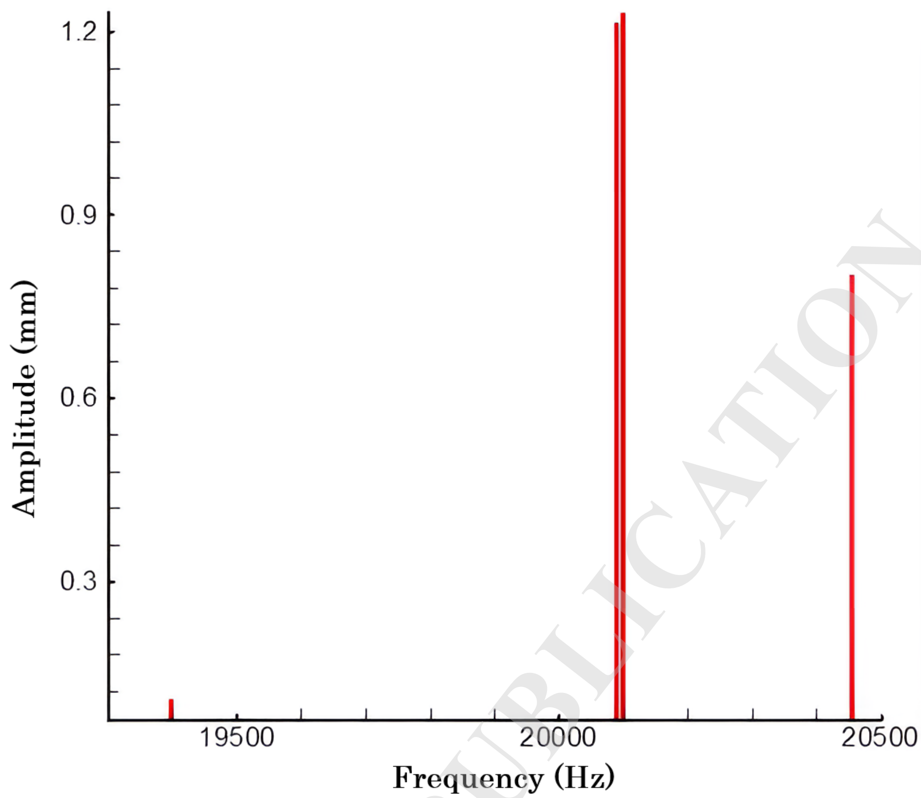

Fig. 6. Distribution of natural frequencies of the flat circular extensive radiator.

3.2. A circular plate with stepped profile

The introduction of stepped profile for a circular radiator (as shown in Fig. 7) can effectively improve the vibrating behavior of the ultrasonic radiating surface (Gallego-Juarez, 2010). The annular grooves with specified depths desirably shift the initiation points of neighboring waves and allows for modification of the radiations. The compensation of counter-phase vibrations of a flat plate is well depicted in Fig. 8. By this approach, it would be possible to design appropriate extensive radiators for different ultrasound applications.

Fig. 7. A circular radiating plate with stepped profile in an airborne ultrasonic system

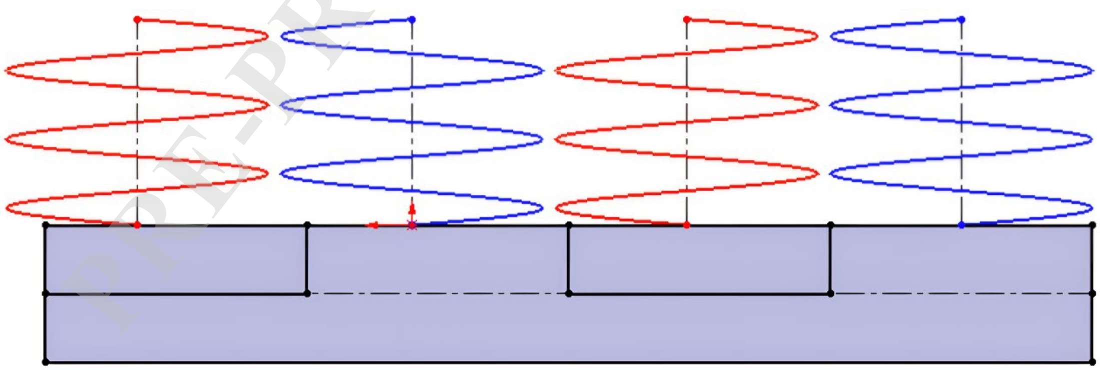

(a)

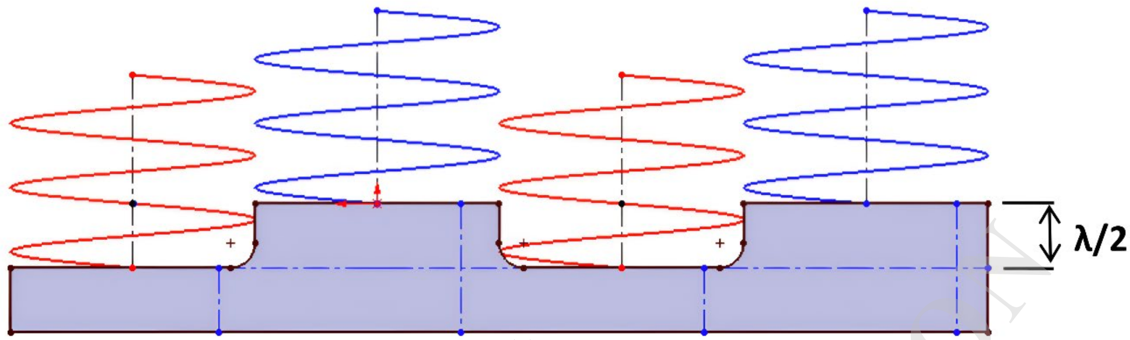

(b)

Fig. 8. (a) Tuning the vibration of different plate zones by using the stepped configuration for the radiating plate (b) the thickness difference between two adjusting zones.

Fig. 9 illustrates the cross-sectional area of an ultrasonic stepped circular radiator. As can be seen, in a stepped profile the selected number of nodal lines divide the plate into several vibrating zones. Throughout the plate, the thickness shift $h_i \quad (i = 1, 2, 3, ..., n)$ is determined according to the wavelength of radiations λ in the medium. Notice that the thickness of plate shifts by half of wave length between two adjusting zones (Fig. 8 b), that is

$$h_i - h_{i-1} = \frac{\lambda}{2} \tag{11}$$

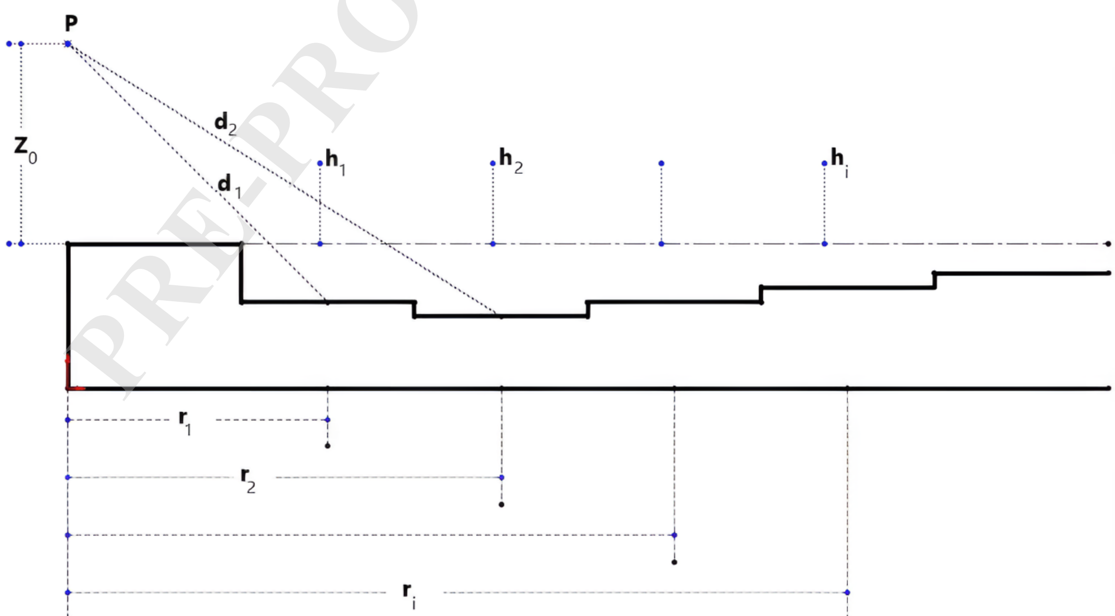

Fig. 9. Geometrical dimensions of a circular stepped plate.

By this consideration, in-phase vibrations will be achieved and the radiated energy focuses on an area around the arbitrary point P. The thickness change in each vibrating zone is determined from the following equation

$$r_i = \sqrt{d_i^2 - (h_i + z_0)} \quad (12)$$

where z_0 is the normal distance of focal point P from the center of plate, r_i is the radius of nodal line and d_i denotes the distance center of plate zone from the point P (see Fig. 9).

In the laboratory setup, the designed radiating plate is installed on the side wall of the drying chamber facing directly to the samples. As a result, the repeated compressions and expansions caused by the ultrasound would enhance the flow-out of moisture from the sample. The radiating plate, however, should be mechanically isolated from the chamber walls to prevent the transmission of vibrations to the structure and minimize the power loss. In the convective drying systems, the plate should be aligned with the direction of hot-air flow to increase the turbulence and reduce the boundary layers against the internal migration of the moisture. According to the results of empirical investigations, the ultrasound drying systems with circular stepped plate radiators have provided significant contributions to hot-air drying of orange peel (Garcia-Perez et al., 2012), strawberries (Gamboa-Santos et al., 2014), persimmon (Cárcel et al., 2007) , clip fish (Bantle & Hanssler, 2013) and peas (Bantle & Eikevik, 2011). The convenient design of radiator profile is very important for radiating focused and high-quality acoustic waves; otherwise, the radiator insufficiently transforms the amplitude of waves generated by the piezo-electric transducer and diminished the overall performance of drying system (Seah et al., 1993).

3.3. Finite element analysis

As mentioned earlier, the application of annular grooves for the extensive plate radiator allows for emitting a highly directive coherent ultrasound waves, essential for a more efficient performance of the system. In this regard, the location of nodal planes is emerged as very important parameters in the design of stepped plate radiators. Based on equations (11) and (12) a one - quarter symmetry sector (shown in Fig. 10a) was developed and used to prepare a three-dimensional graphical model of stepped plate radiator. As can be observed, five nodal lines are selected for the stepped structure for achieving in-phase ultrasonic radiations.

In order to evaluate the effectiveness of proposed design, a FEM model is developed for the modal analysis of the ultrasound system under resonance conditions. Compared with a flat radiator, the stepped profile generates a more complicated geometry. So, the model was meshed by curvature-based elements for appropriate discretizing the grooved and curved boundaries of the stepped circular radiator. The finite element mesh generated for the modal analysis of stepped radiator is shown in Fig. 10b. In order to decrease the computational cost of analysis, less number of Jacobean points were used to study the vibrational behavior as well as the nearby vibration modes at the resonance frequency of the transducer.

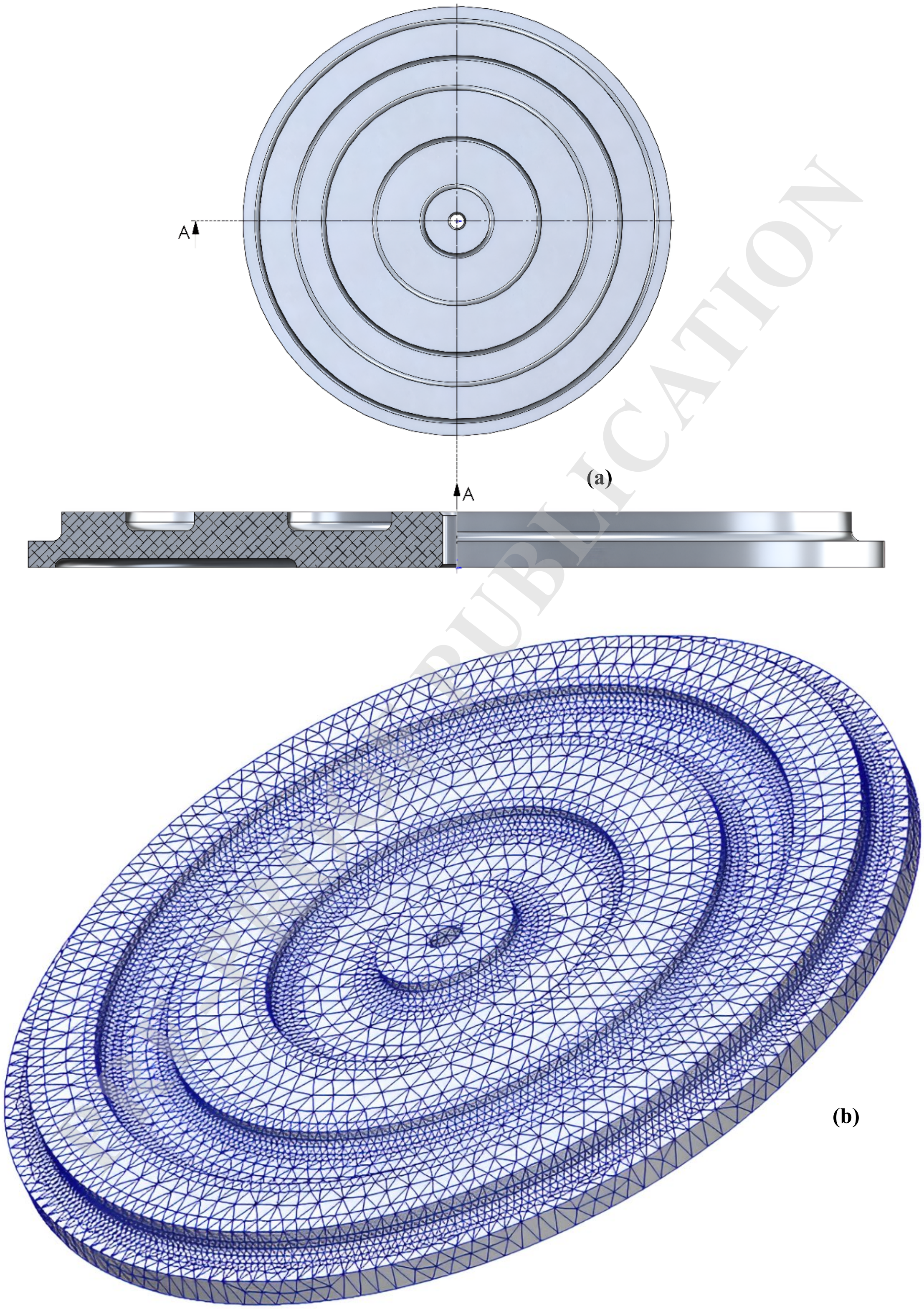

Fig. 10. (a) the dimensions of plate section, (b) the finite element simulation of stepped plate radiator.

For achieving acceptable and accurate numerical predictions, high enough number of nodes and elements should be employed for meshing the domain of problem. However, the excess use of nodes just increases the computational cost and higher round-off errors diminishes the contribution of increased efforts. The convergence analysis is therefore necessary to study the effects of mesh density and developing optimum FEM investigation. The analysis is performed by systematically increase of elements. However, it is well noted that the geometrical discontinuities in radial direction have the most severe effects on the numerical results for natural frequencies. So, instead of global increase in the number of elements, the mesh is first refined in the radial direction. After stabilizing the outputs, the results are then more improved by slightly increase in the number of elements in the thickness direction. In this regard, nine different meshes with specifications given in Table 2, were examined for modal analysis of the circular radiator. It is evident that by increasing the number of nodes, the completion time for meshing as well as conducting each run drastically increases and it is essential to avoid unnecessary nodes and elements. The convergence study continues until stabilization of results in a way that the change in a natural frequency associated with a specific mode shape would be less than 0.1 % between the successive meshes. As mentioned earlier in section 3.1, the axisymmetric mesh is used in this study for discretization of domain of the problem. In this special mesh the number of integration points has a same level of importance as the size of mesh. So, in each considered mesh two runs are conducted for reduced integration points i.e. 2×2 Gaussian points, and full integration points i.e. 2×2 Gaussian points. Then the convergence is concluded from both mesh refinement and insensitivity of the results to the number of integration points. The variation of three natural frequencies of stepped plate radiator with increasing number of nodes is depicted in Fig. 11. Fortunately, the final results namely, 19285, 20259 and 21418 Hz, are very close to the resonance condition of the ultrasonic wave generator (20 kHz) and this is a very good indicator that the dimensions selected in Fig. 10a were selected properly. Fig. 11 also shows that the sparse meshes could not provide accurate results, but by employing less than 15000 elements, all three natural frequencies perfectly converged to their final asymptotic values and this is recognized as the optimum meshing generated for the analysis of the considered problem.

Table 2. Several meshing examined in the convergence analysis

	1	2	3	4	5	6	7	8	9
Max Element Size (mm)	19.02	16.40	13.79	10.94	8.92	7.61	6.18	5.35	4.76
Min Element Size (mm)	6.34	5.46	4.60	3.65	2.97	2.54	2.06	1.78	1.59
Total nodes	3834	4918	6789	10704	23366	33870	54555	75606	119160
Total elements	1826	2361	3284	5270	13446	19969	32338	45399	75331
Maximum Aspect Ratio	12.07	10.67	8.83	8.28	9.48	7.31	6.95	6.73	6.70
Mesh completion time (sec)	12	18	50	93	123	157	254	303	360

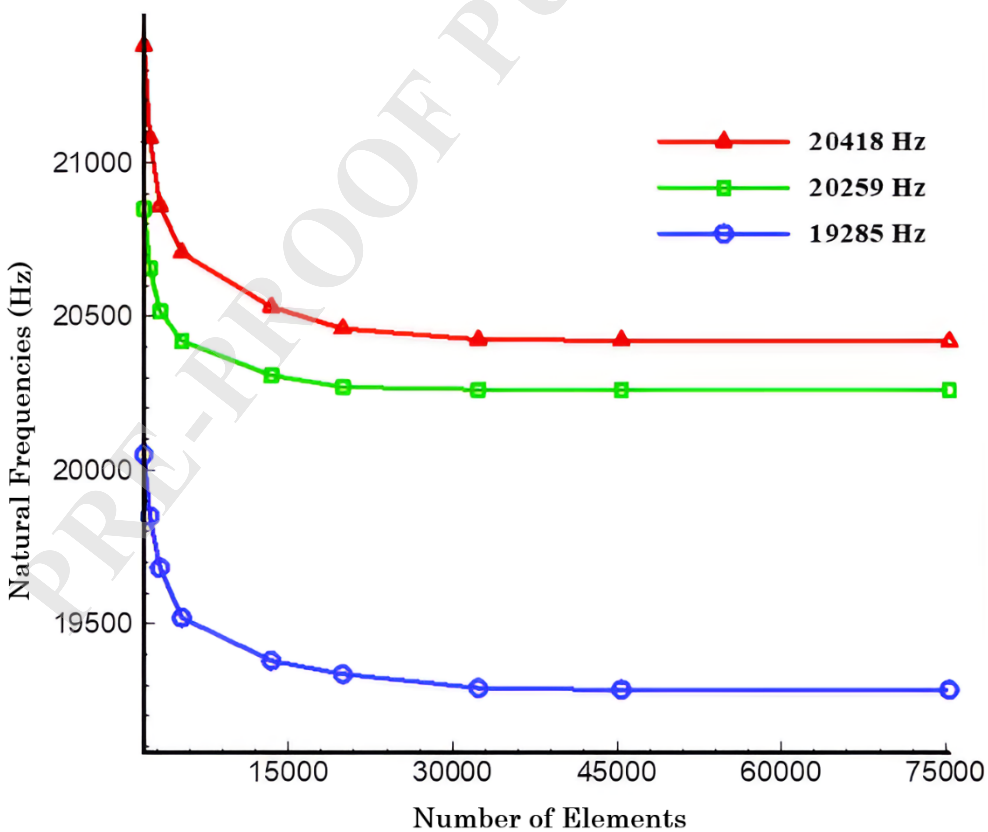

Fig. 11. The effect of mesh density on the convergence of numerical results.

The oscillating behavior of the operating radiator is basically influenced by the mode shapes. Therefore, corresponding to some natural frequencies nearby the resonance condition of the piezo-electric wave generator, the mode shapes were evaluated and the result were given in Fig. 12. It is clear that most of the mode shapes are still counter-phase and found to be similar to those evaluated in Fig. 5 for the flat plate radiator. However, for the natural frequency 20,259 Hz the circular stepped plate showed an outstanding in-phase vibrations which is extremely desired for an excited ultrasonic radiator. This significant modification was just achieved by introduction of stepped profile for the radiating circular plate. So, it is noted that the geometric design procedure used in this study, could provide great facilitation in developing a more convenient and applied ultrasonic system. In special case of drying application, the more focused and powerful propagations from such configuration, can significantly improve the effective moisture diffusivity during the convective dehydration process.

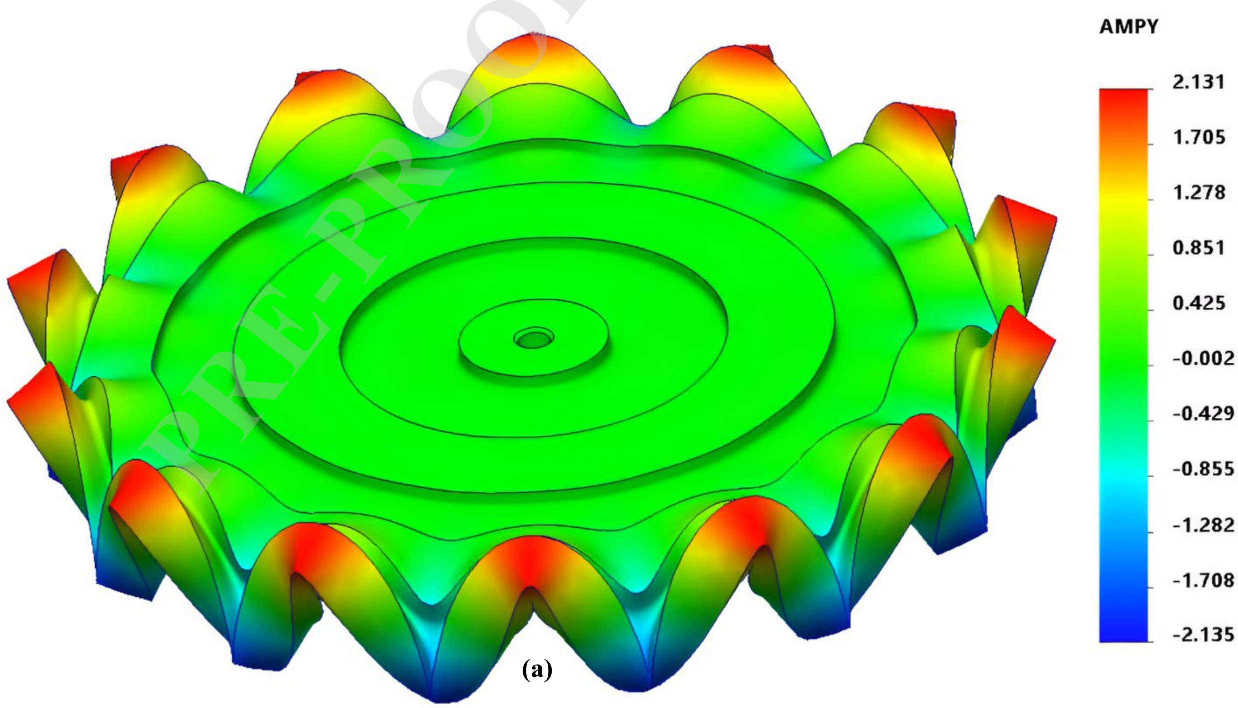

(a)

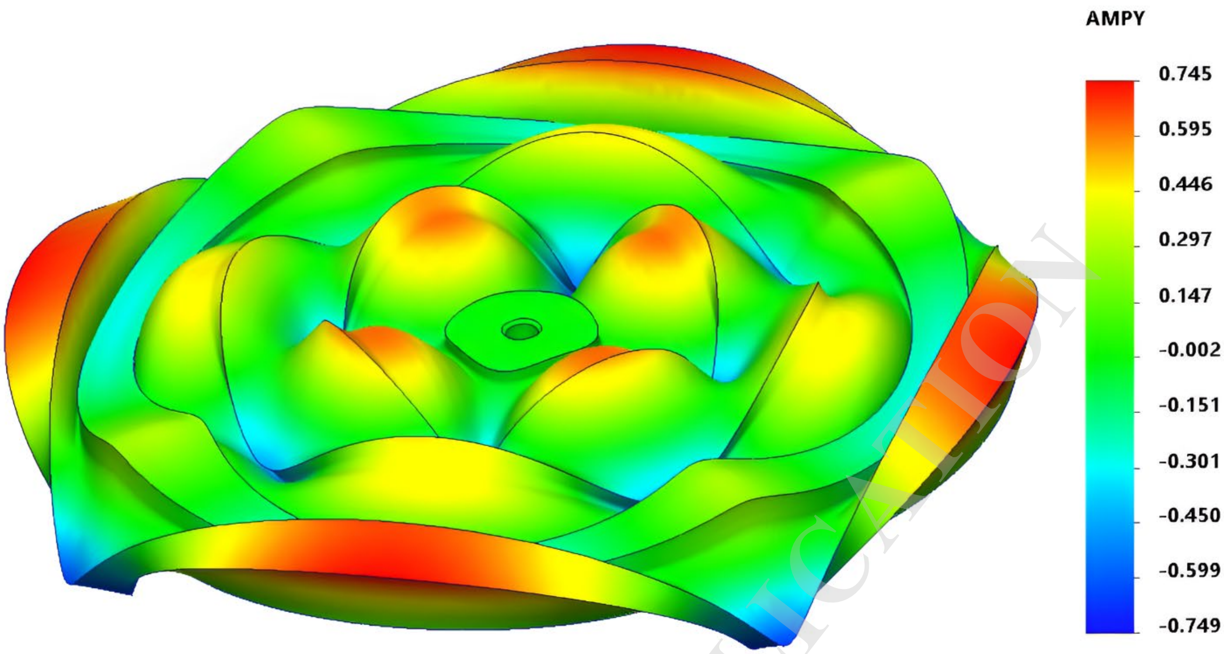
AMPY
0.745
0.595
0.446
0.297
0.147
-0.002
-0.151
-0.301
-0.450
-0.599
-0.749

(b)

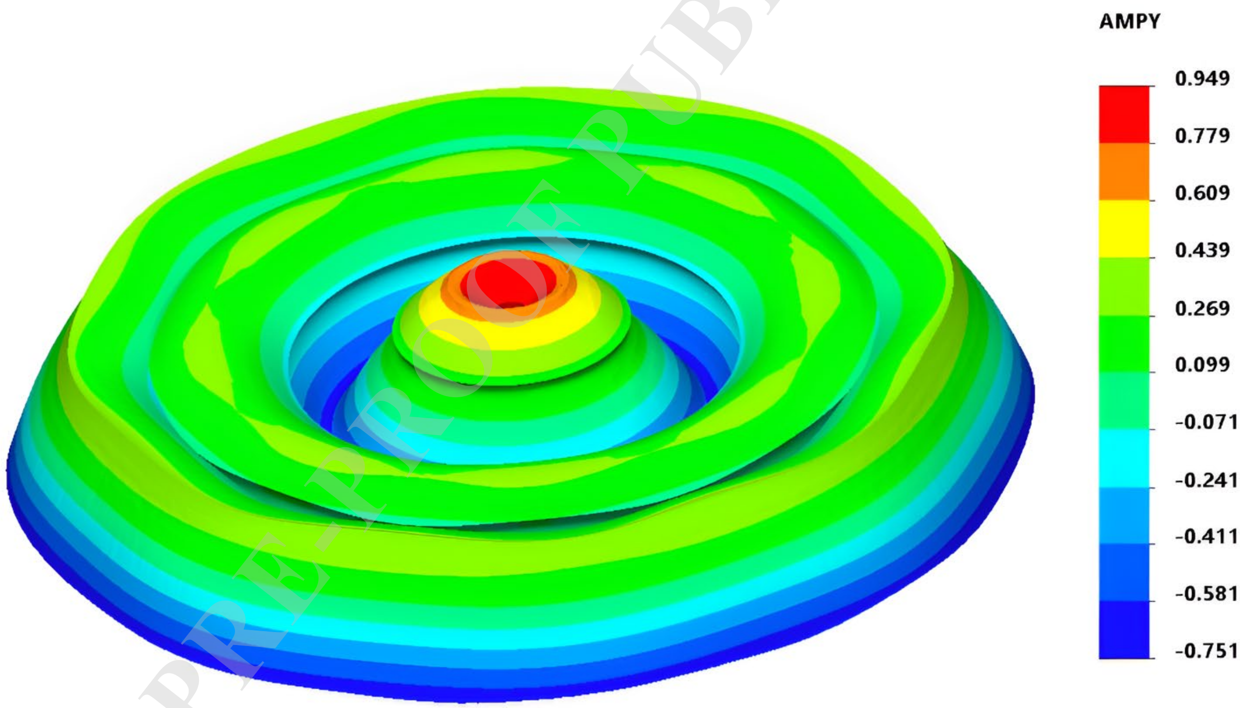
AMPY
0.949
0.779
0.609
0.439
0.269
0.099
-0.071
-0.241
-0.411
-0.581
-0.751

(c)

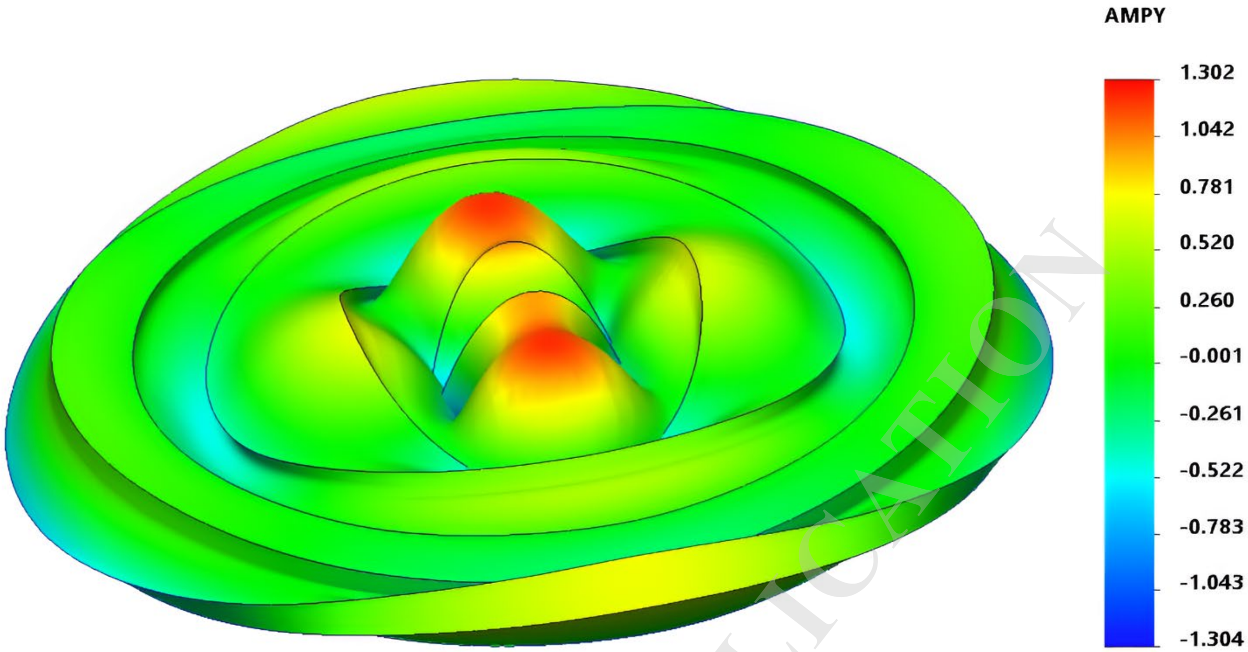

(d)

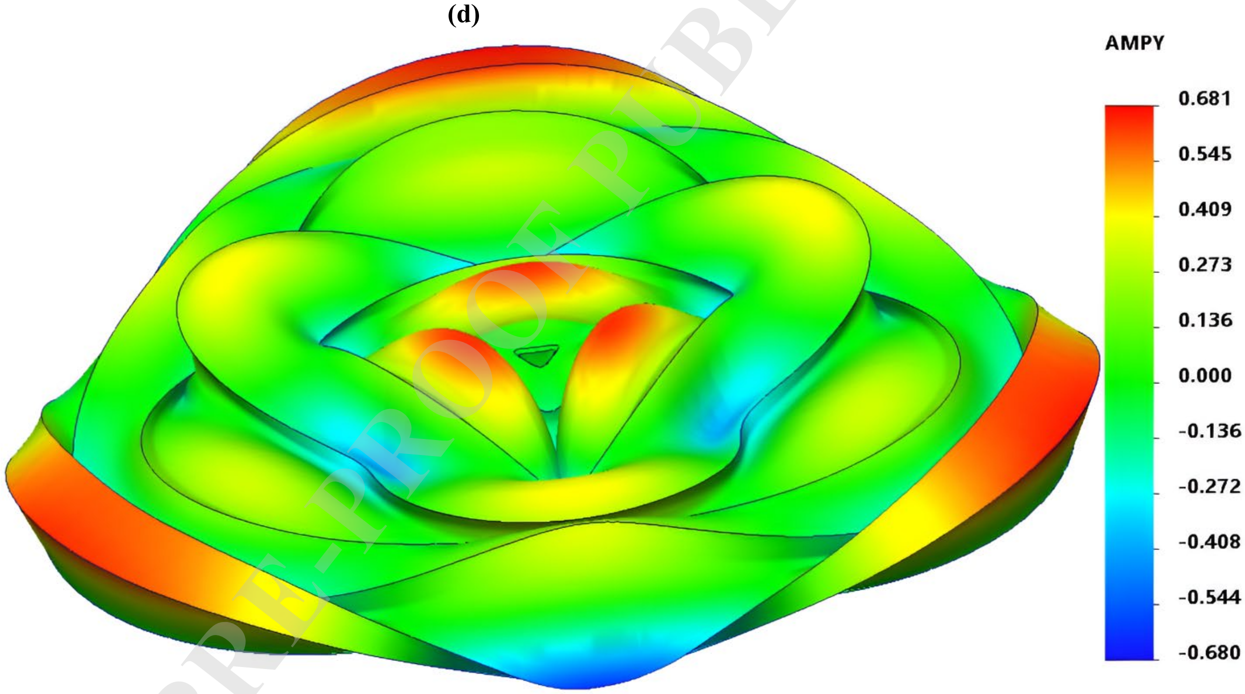

(e)

Fig. 12. The mode shapes of extensive stepped circular radiator at different natural frequencies: (a) 19032 Hz, (b) 19285 Hz, (c) 20,259 Hz, (d) 20,418 Hz, (e) 20,680 Hz.

The distribution of natural frequencies of the stepped radiating surface is another important issue about the proposed design which is depicted in Fig. 13. As can be observed, the mode shapes are quite different, but there is a sufficient gap between the natural frequencies. As a result, the risk of modal interaction during the operation of system is absolutely avoided. This assures a safe operation and effective propagation of high-power ultrasonic waves.

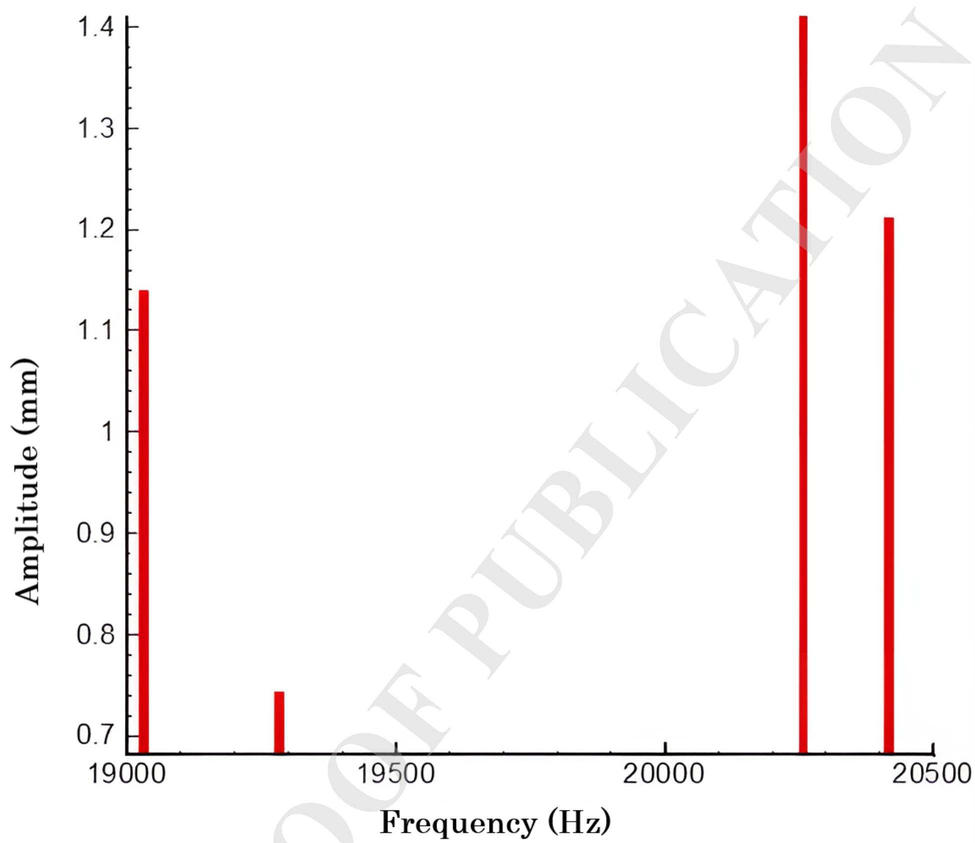

Fig. 13. Distibution of natural frequencies of the stepped circular extensive radiator.

The distribution of amplitudes of the vibrating stepped circular plate at the frequency of 20,259 Hz is shown in Fig. 14. It is evident that the center of plate radiator endures more intense vibrations compared with the points located on the outer areas. This is in a good agreement with the assumptions considered in Fig. 2 for the boundary conditions of the plate for deriving the close-form analytical solution (5). The higher flexural amplitudes at the central part of the plate conveniently enables the radiator to focus the oscillations of the transducer, on a specific point P (see Fig. 9) and intensify the effect of airborne ultrasound on improving the drying process. This mode of vibration is found to be very similar to the oscillating performance of optimized circular plate optimized by Selicani et al. (2021) for ultrasound-assisted drying of carrot.

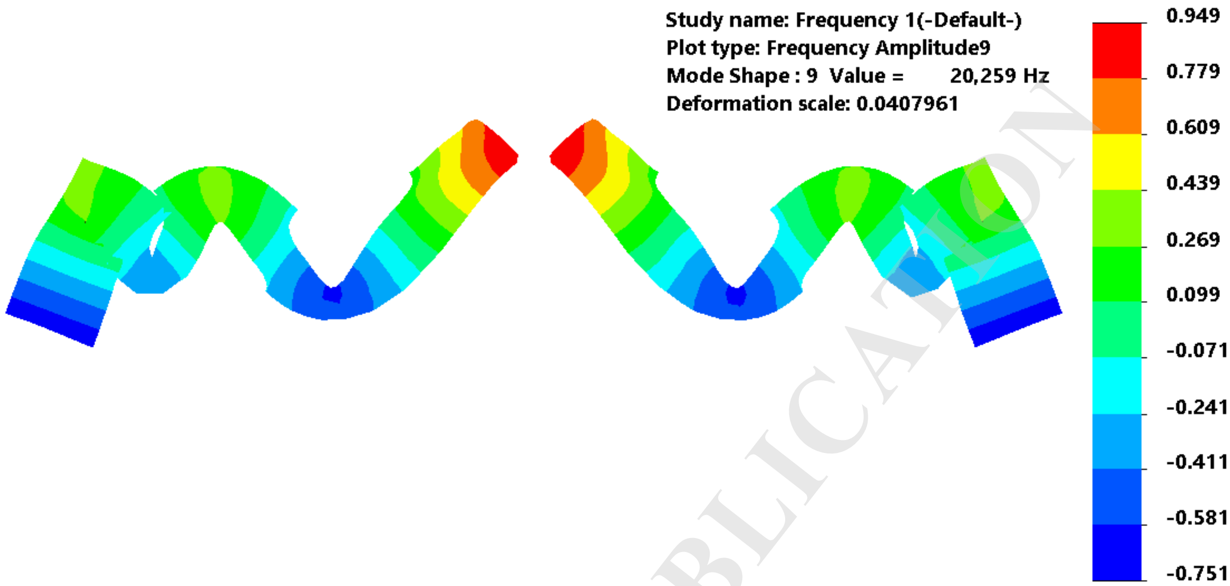

Fig. 14. The amplitudes distribution of the stepped radiator at natural frequency of 20,259 Hz.

Conclusions

In any airborne ultrasound application, there is a considerable impedance mismatch between the wave generating system and the surrounding airflow which diminishes the positive effects of high power waves. Therefore, the piezo-electric transducer should be equipped with an extensive radiating plate to improve the power capacity of the ultrasound system. For drying applications, the frequency of generated ultrasound waves is commonly selected to be 20 kHz. In this case the radiator as a necessary component of the system, should be resonant at this frequency and propagate consistent waves in the gaseous medium. In this study, the results of an analytical solution were used to find the proper geometrical values for a flat circular plate radiator. Then a FEM model is developed for the analysis of proposed design. The model showed that an excited flat radiator endured huge counter-phase radiations with adverse effects on overall performance of the system. So, a stepped profile with proper dimensions was designed to synchronize the vibration of different zones of the circular plate. The modal analysis showed that the geometrical design resulted in a very good mode shape at 20,259 Hz just near the nominal working frequency of the wave generator. Furthermore, the gap between the natural frequencies of the stepped plate was significantly modified by the proposed design to eliminate the risk of modal interaction.

Funding

This research did not receive any specific grant from funding agencies in the public, commercial, or not-for-profit sectors.

Conflicts of interest

The authors declare that they have no known competing financial interests or personal relationships that could have appeared to influence the work reported in this paper.

Data availability statement

The data that support the findings of this study are available from the corresponding author upon reasonable request.

Author contribution statement

Hossein Golbakhshi: Preparation, Writing- Original draft. **Moslem Namjoo:** Methodology, Software, Data curation, Formal analysis.

References

Amin, S., Ahmed, M., & Youssef, H. (1995). Computer-aided design of acoustic horns for ultrasonic machining using finite-element analysis. *Journal of Materials Processing Technology*, *55*(3-4), 254–260. https://doi.org/https://doi.org/10.1016/0924-0136(95)02015-2

Andres, R., Acosta, V., Lucas, M., & Riera, E. (2018). Modal analysis and nonlinear characterization of an airborne power ultrasonic transducer with rectangular plate radiator. *Ultrasonics*, *82*, 345–356. https://doi.org/https://doi.org/10.1016/j.ultras.2017.09.017

Bantle, M., & Eikevik, T. M. (2011). Parametric study of high-intensity ultrasound in the atmospheric freeze drying of peas. *Drying Technology*, *29*(10), 1230–1239. https://doi.org/https://doi.org/10.1080/07373937.2011.584256

Bantle, M., & Hanssler, J. (2013). Ultrasonic convective drying kinetics of clipfish during the initial drying period. *Drying Technology*, *31*(11), 1307–1316. https://doi.org/https://doi.org/10.1080/07373937.2013.792093

Cárcel, J., García-Pérez, J., Riera, E., & Mulet, A. (2007). Influence of high-intensity ultrasound on drying kinetics of persimmon. *Drying Technology*, *25*(1), 185–193. https://doi.org/https://doi.org/10.1080/07373930601161070

Ensminger, D. (1988). *Ultrasonics: fundamentals, technology, applications, revised and expanded*. CRC press.

Fernandes, F. A., Rodrigues, S., García-Pérez, J. V., & Carcel, J. A. (2016). Effects of ultrasound-assisted air-drying on vitamins and carotenoids of cherry tomatoes. *Drying Technology*, *34*(8), 986–996. https://doi.org/https://doi.org/10.1080/07373937.2015.1090445

Gallego-Juarez, J. (1989). Piezoelectric ceramics and ultrasonic transducers. *Journal of Physics E: Scientific Instruments*, *22*(10), 804. https://doi.org/https://doi.org/10.1088/0022-3735/22/10/001

Gallego-Juarez, J. A. (2010). High-power ultrasonic processing: recent developments and prospective advances. *Physics Procedia*, *3*(1), 35–47. https://doi.org/https://doi.org/10.1016/j.phpro.2010.01.006

Gallego-Juárez, J. A., Rodríguez, G., Acosta-Aparicio, V. M., Riera, E., & Cardoni, A. (2015). 7 - Power ultrasonic transducers with vibrating plate radiators*. In J. A. Gallego-Juárez & K. F. Graff (Eds.), *Power Ultrasonics* (pp. 159–193). Woodhead Publishing. https://doi.org/https://doi.org/10.1016/B978-1-78242-028-6.00007-7

Gallego-Juárez, J. A., Rodriguez, G., Acosta, V., & Riera, E. (2010). Power ultrasonic transducers with extensive radiators for industrial processing. *Ultrasonics Sonochemistry*, *17*(6), 953–964. https://doi.org/https://doi.org/10.1016/j.ultsonch.2009.11.006

Gamboa-Santos, J., Montilla, A., Soria, A. C., Cárcel, J. A., García-Pérez, J. V., & Villamiel, M. (2014). Impact of power ultrasound on chemical and physicochemical quality indicators of strawberries dried by convection. *Food Chemistry*, *161*, 40–46. https://doi.org/https://doi.org/10.1016/j.foodchem.2014.03.106

Garcia-Perez, J. V., Ortuño, C., Puig, A., Carcel, J. A., & Perez-Munuera, I. (2012). Enhancement of water transport and microstructural changes induced by high-intensity ultrasound application on orange peel drying. *Food and Bioprocess Technology*, *5*(6), 2256–2265. https://doi.org/https://doi.org/10.1007/s11947-011-0645-0

Ghasemi, G., Moradi, M., Zare, D., Golbakhshi, H., & Namjoo, M. (2023). Energy and exergy-based threshold setting for the auxiliary heating source of a hybrid solar/IR drying system. *Sustainable Energy Technologies and Assessments*, *59*, 103400. https://doi.org/https://doi.org/10.1016/j.seta.2023.103400

Golbakhshi, H., Namjoo, M., & Kamandar, M. R. (2024). The Modal and Harmonic Analysis of a Cylindrical Horn Designed for an Airborne Ultrasonic Dryer. *Biomechanism and*

Bioenergy Research, *3*(2), 14–30. https://doi.org/https://doi.org/10.22103/bbr.2024.23407.1084
Han, M., Zhang, G., & Zhang, X. (2024). Study on the radiation directivity of a ring-excited thin circular plate with a fixed boundary. *Ultrasonics*, *144*, 107441. https://doi.org/https://doi.org/10.1016/j.ultras.2024.107441
Huang, D., Men, K., Li, D., Wen, T., Gong, Z., Sunden, B., & Wu, Z. (2020). Application of ultrasound technology in the drying of food products. *Ultrasonics Sonochemistry*, *63*, 104950.
Lei, Y., Wang, W., Zhang, C., Wang, D., Zhuang, W., Zheng, B., Lo, Y. M., & Tian, Y. (2021). Evaluation of the chemical qualities and microstructural changes of Lentinula edodes caused by airborne ultrasonic treatment combined with microwave vacuum drying. *Journal of food science*, *86*(3), 667–676. https://doi.org/https://doi.org/10.1111/1750-3841.15593
Li, M., Zhou, C., Wang, B., Zeng, S., Mu, R., Li, G., Li, B., & Lv, W. (2023). Research progress and application of ultrasonic-and microwave-assisted food processing technology. *Comprehensive Reviews in Food Science and Food Safety*, *22*(5), 3707–3731. https://doi.org/https://doi.org/10.1111/1541-4337.13198
Mason, T. J., Riera, E., Vercet, A., & Lopez-Buesa, P. (2005). Application of ultrasound. In *Emerging technologies for food processing* (pp. 323–351). Elsevier. https://doi.org/https://doi.org/10.1016/B978-012676757-5/50015-3
Matuda, M. Y., & Adamowski, J. C. (1999). Modelagem de transdutores piezelétricos de potência.
Namjoo, M., Dibagar, N., Golbakhshi, H., Figiel, A., & Masztalerz, K. (2024). RSM-Based Optimization Analysis for Cold Plasma and Ultrasound-Assisted Drying of Caraway Seed. *Foods*, *13*(19), 3084. https://doi.org/https://doi.org/10.3390/foods13193084
Namjoo, M., Golbakhshi, H., Kamandar, M. R., & Jahromi, M. S. B. (2026). Performance evaluation using artificial neural network technique and exergetic impact of cold plasma pretreatment on hybrid Ultrasound/Convective drying of ginger slices. *Thermal Science and Engineering Progress*, 104679. https://doi.org/https://doi.org/10.1016/j.tsep.2026.104679
Namjoo, M., Moradi, M., Dibagar, N., & Niakousari, M. (2022). Cold Plasma Pretreatment Prior to Ultrasound-assisted Air Drying of Cumin Seeds. *Food and Bioprocess Technology*, *15*(9), 2065–2083. https://doi.org/10.1007/s11947-022-02863-8
Namjoo, M., Moradi, M., Nematollahi, M. A., & Golbakhshi, H. (2025). Artificial Neural Network (ANN) Modeling of Plasma and Ultrasound-assisted Air Drying of Cumin Seeds. *Journal of Agricultural Machinery*, 1–22. https://doi.org/https://doi.org/10.22067/jam.2024.85744.1209
Namjoo, M., Moradi, M., & Niakousari, M. (2022). Evaluation of the effect of high-power ultrasound waves on conventional air drying of cumin seeds. *Sustainable Energy Technologies and Assessments*, *52*, 102262. https://doi.org/https://doi.org/10.1016/j.seta.2022.102262
Perera, C. O., & Alzahrani, M. A. J. (2021). Ultrasound as a pre-treatment for extraction of bioactive compounds and food safety: A review. *LWT*, *142*, 111114. https://doi.org/https://doi.org/10.1016/j.lwt.2021.111114

Seah, K., Wong, Y., & Lee, L. (1993). Design of tool holders for ultrasonic machining using FEM. *Journal of Materials Processing Technology*, *37*(1-4), 801–816. https://doi.org/https://doi.org/10.1016/0924-0136(93)90138-V
Selicani, G. V., & Buiochi, F. (2021). Stepped-plate ultrasonic transducer used as a source of harmonic radiation force optimized by genetic algorithm. *Ultrasonics*, *116*, 106505. https://doi.org/https://doi.org/10.1016/j.ultras.2021.106505
Staszewski, W., Gudra, T., & Opieliński, K. J. (2018). The acoustic field distribution inside the ultrasonic ring array. *Archives of Acoustics*, *43*(3), 455–463. https://doi.org/https://doi.org/10.24425/123917
Tang, J., Zhu, X., Jambrak, A. R., Sun, D.-W., & Tiwari, B. K. (2024). Mechanistic and synergistic aspects of ultrasonics and hydrodynamic cavitation for food processing. *Critical Reviews in Food Science and Nutrition*, *64*(24), 8587–8608. https://doi.org/https://doi.org/10.1080/10408398.2023.2201834
Tao, Zhang, J., Jiang, S., Xu, Y., Show, P.-L., Han, Y., Ye, X., & Ye, M. (2018). Contacting ultrasound enhanced hot-air convective drying of garlic slices: Mass transfer modeling and quality evaluation. *Journal of food engineering*, *235*, 79–88. https://doi.org/https://doi.org/10.1016/j.jfoodeng.2018.04.028
Tao, Y., Zhang, J., Jiang, S., Xu, Y., Show, P.-L., Han, Y., Ye, X., & Ye, M. (2018). Contacting ultrasound enhanced hot-air convective drying of garlic slices: Mass transfer modeling and quality evaluation. *Journal of food engineering*, *235*, 79–88. https://doi.org/https://doi.org/10.1016/j.jfoodeng.2018.04.028
Timoshenko, S., & Woinowsky-Krieger, S. (1959). Theory of plates and shells.
Vallespir, F., Rodríguez, Ó., Cárcel, J. A., Rosselló, C., & Simal, S. (2019). Ultrasound assisted low-temperature drying of kiwifruit: Effects on drying kinetics, bioactive compounds and antioxidant activity. *Journal of the Science of Food and Agriculture*, *99*(6), 2901–2909. https://doi.org/https://doi.org/10.1002/jsfa.9503
Xu, B., Tiliwa, E. S., Yan, W., Azam, S. R., Wei, B., Zhou, C., Ma, H., & Bhandari, B. (2022). Recent development in high quality drying of fruits and vegetables assisted by ultrasound: A review. *Food Research International*, *152*, 110744. https://doi.org/https://doi.org/10.1016/j.foodres.2021.110744
Xu, J., Wang, D., Lei, Y., Cheng, L., Zhuang, W., & Tian, Y. (2022). Effects of combined ultrasonic and microwave vacuum drying on drying characteristics and physicochemical properties of Tremella fuciformis. *Ultrasonics Sonochemistry*, *84*, 105963. https://doi.org/https://doi.org/10.1016/j.ultsonch.2022.105963
Zhou, S., Chen, W., Chitrakar, B., & Fan, K. (2024). Ultrasound technology for enhancing drying efficiency and quality of fruits and vegetables: A review. *Food and Bioprocess Technology*, *17*(12), 4506–4536. https://doi.org/https://doi.org/10.1007/s11947-024-03379-z